MDPI

Article

Early Triassic Monzonite–Granite Series in Eastern Kazakhstan as a Reflection of Siberian Large Igneous Province Activity

Sergey V. Khromykh [1,*], Pavel D. Kotler [1,2,3], Anna V. Kulikova [1,3], Dina V. Semenova [1,3], Kamil R. Minnebaev [3], Bulat I. Gareev [3], Georgii A. Batalin [3], Tatiana N. Antsiferova [4,5], Ekaterina A. Il'icheva [1,2] and Alexey S. Volosov [1,2]

[1] V.S. Sobolev Institute of Geology and Mineralogy, Siberian Branch of Russian Academy of Sciences, 3 Koptyug Ave., 630090 Novosibirsk, Russia
[2] Department of Geology and Geophysics, Novosibirsk State University, 1, Pirogova 1 Str., 630090 Novosibirsk, Russia
[3] Institute of Geology and Petroleum Technology, Kazan Federal University, 18, Kremlyovskaya Str., 420008 Kazan, Russia
[4] Institute of Geology of Ore Deposits, Petrography, Mineralogy and Geochemistry, Russian Academy of Sciences, 35 Staromonetny Per., 119017 Moscow, Russia
[5] Institute of Volcanology and Seismology, Far East Branch of Russian Academy of Sciences, 9 Piip Boulevard, 683006 Petropavlovsk-Kamchatsky, Russia
* Correspondence: serkhrom@igm.nsc.ru; Tel.: +7-913-909-30-79

Abstract: We provide the results of studying the internal structure and composition of the rocks of the Semeitau and Delbegetei massifs located in Eastern Kazakhstan. It was previously believed that these massifs have different ages and were formed in different geodynamic settings. The U-Pb zircon age from the monzonites and quartz monzonites was determined to be 249 ± 2 Ma, which showed the same Early Triassic age of the massifs. Both massifs are composed of rocks of the same monzonite–granite series of rocks with a significant proportion of high-silica rocks (leucocratic granites). Intermediate rocks are formed due to the differentiation of subalkaline mafic magmas, and the felsic rocks (rhyolites and granites) are the result of partial melting of crustal substrates. The massif formation model assumes the intrusion of mafic magmas into the crust, their differentiation and mixing with crustal melts, and then the intrusion of various rocks into the upper crustal levels. Analysis of the geological position, age and composition of the rocks allows us to conclude that the Semeitau and Delbegetei massifs were formed in an intraplate geodynamic setting. The activity of the mantle plume is the most probable reason for their formation. The Semeitau and Delbegetei massifs can be included in the southern part of the range of the Early Triassic Siberian Large Igneous Province.

Keywords: monzonites; granites; Early Triassic magmatism; Siberian Large Igneous Province; Eastern Kazakhstan

1. Introduction

Large Igneous Provinces (LIPs) are huge-volume, short-duration pulses of intraplate magmatism that can produce igneous volumes that can compete with or even outstrip those produced at subduction zones [1–3].

Siberian LIP is one of the largest provinces; a huge burst of magmatism is associated with its activity [4–8], etc. Basalt covers and sills occupy a huge part of the Siberian Platform; they are also widespread under the cover of the Mesozoic–Cenozoic West Siberian Basin and associate with rift structures. In addition to basalts, many Permian–Triassic intrusive complexes are associated with the Siberian LIP [9–11]. This makes it possible to delineate the zone of the Siberian LIP influence in Eurasia (Figure 1). In the south, the area of distribution of Permian–Triassic magmatism was drawn along the southern boundary of the West Siberian Basin [5]. Recently, more information about the manifestation of Late Paleozoic–Early Mesozoic magmatism within the Central Asian Orogenic Belt was

obtained [10,12,13]. Nevertheless, the south boundary of the Siberian LIP influence has not yet been precisely determined. This is one of the principal scientific questions to appreciate the scale of thermal effects from mantle magmas of plume origin on a lithosphere. To solve the question, it is necessary to summarize petrological and geochronological data on many granitoid massifs within southern Siberia and northern Kazakhstan. Such a task requires great effort, and petrological and geochronological data on some individual granitoid massifs can serve as a contribution to its implementation.
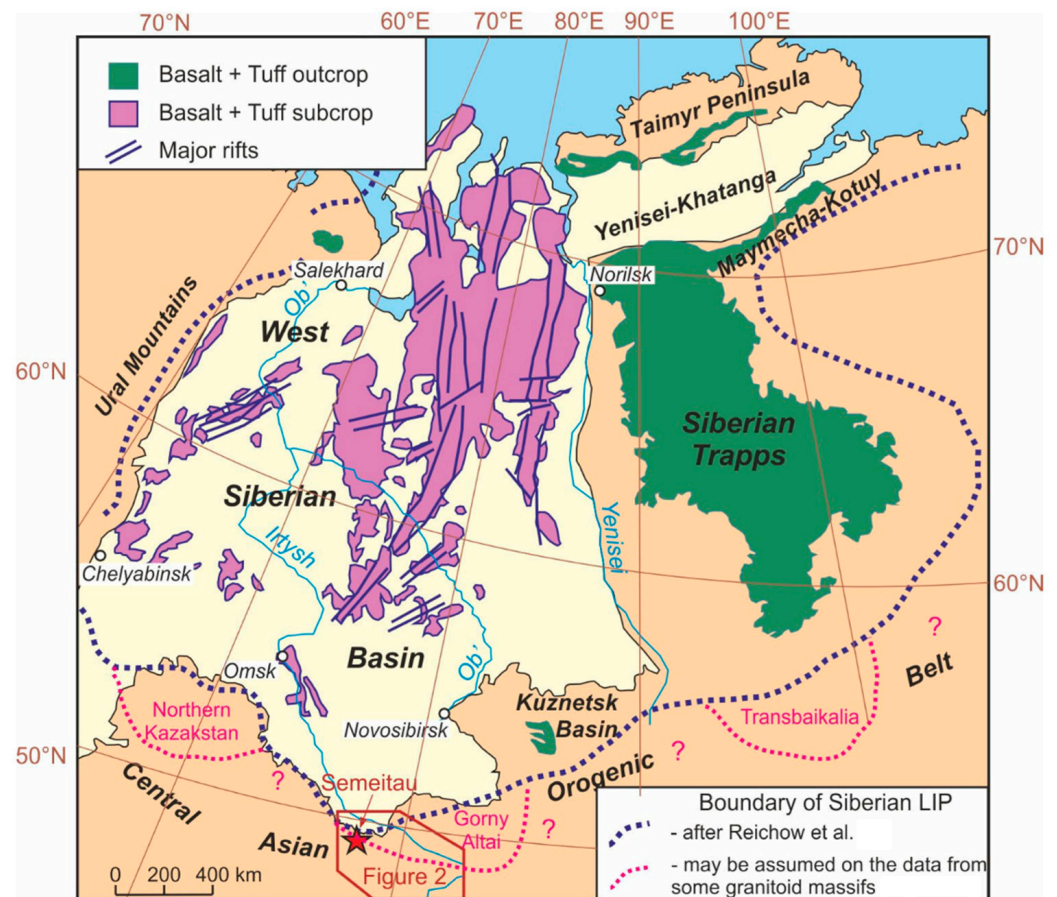

Figure 1. Simplified map of the Siberian Large Igneous Province and the boundary of its manifestation that was presumed before (after [5]) and that may be presumed now (after [10,12], etc.). The "?" means the lack yet of any data about Early Triassic granites in these areas.

One of the examples of such massifs is the Semeitau massif in Eastern Kazakhstan, for which the Early Triassic age was previously established [13]. Our latest petrographic, geochemical, and geochronological data of the Semeitau massif and the nearby Delbegetei massif allowed us to confirm their Early Triassic age and associate them with the Siberian LIP.

2. Geological Background

The Eastern Kazakhstan territory is the unique geologic province with a complex and peculiar history of the formation, where a number of large-scale rare (Li, Be, Ta, Sn), non-ferrous (Cu, Ni, Zn, Pb) and precious (Au, Ag) metal deposits are concentrated [14,15]. The Eastern Kazakhstan area is located in the west of the Central Asian Orogenic Belt (CAOB), and it is part of the Hercynian Ob'–Zaisan folded system. Eastern Kazakhstan region is oriented from northwest to southeast and extends over a length of 700 km. The southwest boundary of Eastern Kazakhstan region is the Chingiz–Tarbagatai regional fault separating it from the Middle Paleozoic rocks of the Kazakhstan continent, and in the northeast, it is bounded by the Irtysh shear zone that separates it from the Middle Paleozoic rocks of the

Rudny Altai margin of the Siberian continent. The folded system in Eastern Kazakhstan was formed during convergence of the Siberian and Kazakhstan continents and Late Paleozoic closure of the Ob'-Zaisan Ocean [16–19]. The general sequence of geodynamic events in Eastern Kazakhstan is as follows: subduction → convergence of continental blocks and reduction in the ocean basin → termination of marine sedimentation and basin crowding → orogeny with tectonic growth of the sedimentary section and subsequent appearance of continental molasses → extension and orogen collapse [17,18,20]. This gives ground to classify the geological structure of the region as an accretion–collision system.

All stages of the accretion–collision system development of the Eastern Kazakhstan were accompanied by characteristic manifestations of mafic and granitoid magmatism. The early orogenic stage of the late part of the Early Carboniferous includes the gabbro-diorite–granitoid intrusions of the Saur Series, the formation of which is associated with the slab break-off [20,21]. At the late orogenic stage during the Middle–Upper Pennsylvanian in the Eastern Kazakhstan intracontinental basalt–andesitic volcanism [22], few dike swarms [21] and ultramafic–mafic intrusions [23] were formed. The granitoid magmatism of this stage is represented by dacite and rhyolite troughs [24] and small intrusions of K-Na- and Na-granitoids [25]. The intrusions of this stage are confined to regional faults. We assume that their formation is related with late collisional extension associated with shear motions.

The most large-scale magmatism in Eastern Kazakhstan manifested in the Early Permian, after the completion of orogenic processes. Our latest petrological and geochronological studies have established the Early Permian age of most of the igneous associations shown in Figure 2.
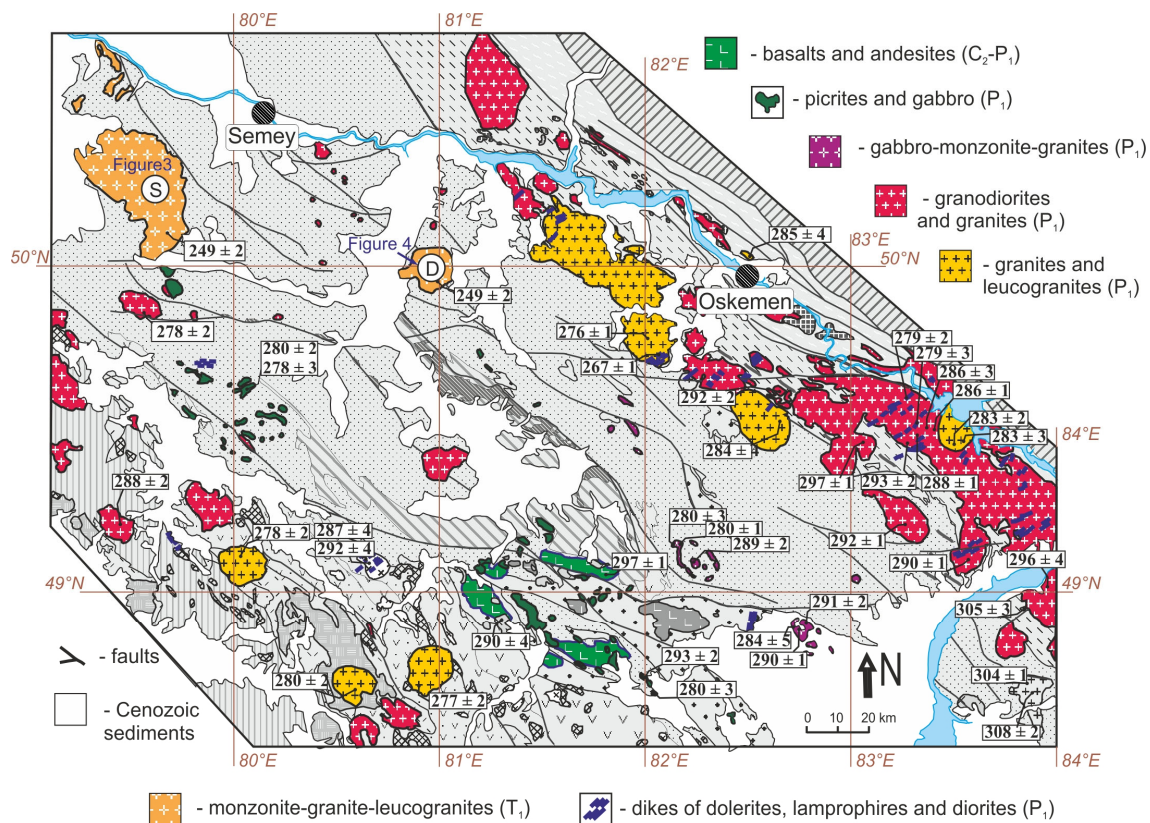
Figure 2. Scheme of location of igneous complexes of Late Carboniferous (C_2), Early Permian (P_1) and Early Triassic (T_1) age in the territory of Eastern Kazakhstan. Numbers in the rectangles indicate the determined age (U-Pb data on zircons) of the igneous rocks, from [20]. Previous sedimentary, volcanic and intrusive formations (age range from Silurian to Late Carboniferous) are shown in shades of gray. A more detailed map is published in [20]. "S" denotes the Semeitau massif, "D" denotes the Delbegetei massif.

In the early Permian, the following rock types were intruded:

- massifs of picrites and gabbro, 290–280 Ma [26];
- multiphase gabbro-diorite-monzonite–granite–leucogranite intrusions [27];
- large massifs of granodiorite–granites composing batholiths [28–30];
- large granite–leucogranites massifs [29];
- dyke swarms of dolerites, lamprophyres and diorites [31,32].

The geological relationships and composition of these rock associations have been compared in a recent summary work [20]. It was shown that mafic igneous complexes with enriched geochemical characteristics correspond to within-plate settings. The subcontinental lithospheric mantle could be the source of these magmas. In the same work [20], the volume of Early Permian granitoids on the territory of Eastern Kazakhstan was estimated as 100,000–150,000 km^3 [20]. Early Permian (300–270 million years ago) mafic magmatism and large volumes of granitoids were manifested in vast areas in Kazakhstan, northwest China, Kyrgyzstan, Uzbekistan and southwestern Mongolia [33–44], etc. A plume-related trap basalt formation was formed at that time in the Tarim Craton [45–47], etc. Extensive Early Permian magmatism was combined into the Early Permian Tarim large igneous province formed during the Tarim mantle plume activity [3,40,42,48–53]. Thus, the most large-scale magmatism in the territory of Eastern Kazakhstan is the result of the activity of the Tarim LIP [20,53].

Having obtained evidence of the Early Permian age of most igneous associations of Eastern Kazakhstan, we believed that igneous activity in this area was finished at the late part of the Early Permian. This aroused our interest in studying the rocks of the Semeitau massif, to confirm or deny their previously assumed Triassic age [14,54–56]. Our data of the Semeitau massif and the nearby Delbegetei massif allowed us to confirm their Early Triassic age. The obtained data became the basis for this article.

3. Semeitau and Delbegetei Massifs—Geological Structure

The Semeitau massif is oriented from the northwest to the southeast and stretches for about 45 km, and from the southwest to the northeast for about 25 km (Figure 3), located among the Early Carboniferous (Tournais-Vize) terrigenous–carbonate sedimentary rocks (sandstones and siltstones with lenses and blocks of limestone). A large part of the massif is covered with loose Quaternary sediments. Nevertheless, a sufficient amount of igneous rocks is exposed as small mountain ridges rising tens of meters above the steppe. This allowed the predecessors to study in detail the internal structure of the massif in the 1960s and 1970s [54,55] and to determine two stages of the igneous history.

Volcanic rocks of the first stage are first basalts, then trachytes and quartz trachytes, and then rhyolites. These rocks are exposed in the southern and southeastern parts of the massif. Basalts and trachytes are rare. Rhyolites and rhyolite ignimbrites up to 200 m thick in some parts of the structure are predominant and contain xenoliths of early basalts, trachytes and sedimentary rocks. At the base of the rhyolitic section, interlayers and lenses of tuffs and siltstones were found with identified plant fossil from the Lower Triassic [54]. This fact has traditionally been a geological proof of the Triassic age of the Semeitau massif.

The second stage of magmatism includes subvolcanic and hypabyssal intrusive rocks. It is represented by monzonites, syenites, granosyenite–porphyries and granite–porphyries. Monzonites form some isometric bodies in the central and eastern parts of massif. Monzonites are intruded by dikes of fine-grained syenites. Granosyenite–porphyries comprise two large bodies in the northeast and northwest of the Semeitau massif (see Figure 3). They are not in contact with monzonites, but are similar in composition to syenitedikes-intruding monzonites. The subvolcanic granite–porphyries are distributed in the central, western, and northwestern parts of the Semeitau structure. The latest igneous bodies are a few dolerite dikes intruding monzonites in the central part of the massif and quartz syenites in the northeastern part of the massif. The dikes are tens of meters long and one meter wide.

The Delbegetei massif has a shape close to isometric with a diameter of about 15 km. The igneous rocks of the massif form igor, rising tens of meters above the surrounding

steppe. The mountains are cut by valleys filled with Quaternary sediments (Figure 4). The massif intrudes polymictic sandstones, gravelstones, and siltstones of Carboniferous age. A detailed study of the massif in the 1960s and 1970s [55] made it possible to identify several intrusive phases. Quartz monzonites as small bodies are found in the western ledge of the massif, representing the first intrusive phase.
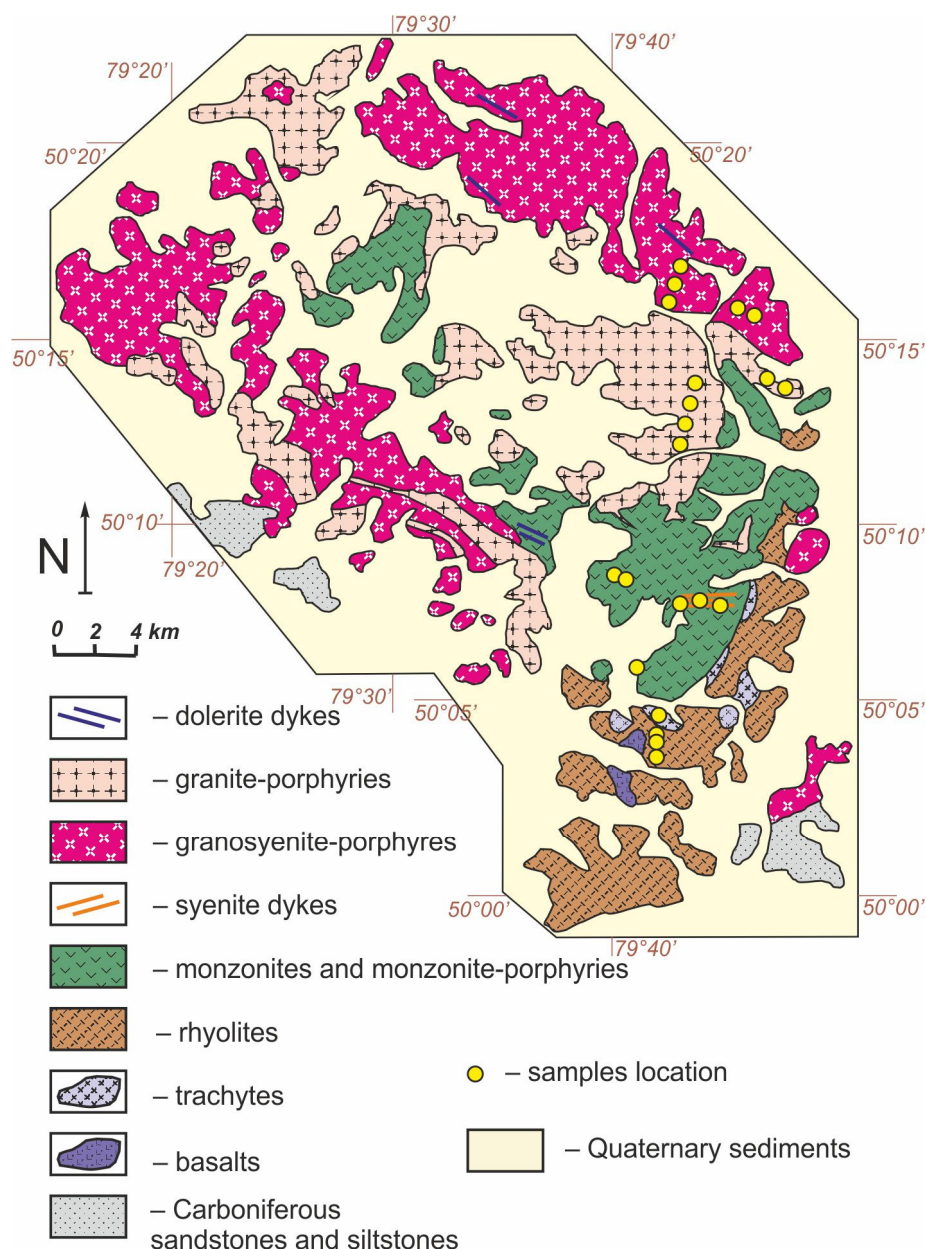
Figure 3. Geological map for Semeitau massif, after [55].

Biotite granites and leucocratic granites are the next intrusive phase, but the relationship between these intrusive phases has not been fully elucidated. It is generally accepted that porphyritic granites are intruded earlier than medium-grained equigranular granites, and that fine-grained granites are the youngest. Thus, it is assumed that porphyritic granites are assigned to second phase, medium-grained granites are assigned to third phase, and fine grained granites are assigned to fourth phase (see Figure 4).

Figure 4. Geological map for Delbegetei massif, after [55].

4. Materials and Methods

This study reports field observations and analytical work. More than 80 samples were collected from bedrock exposures. The sample locations are given in Figures 3 and 4 and are given in the Supplementary Kml-file.
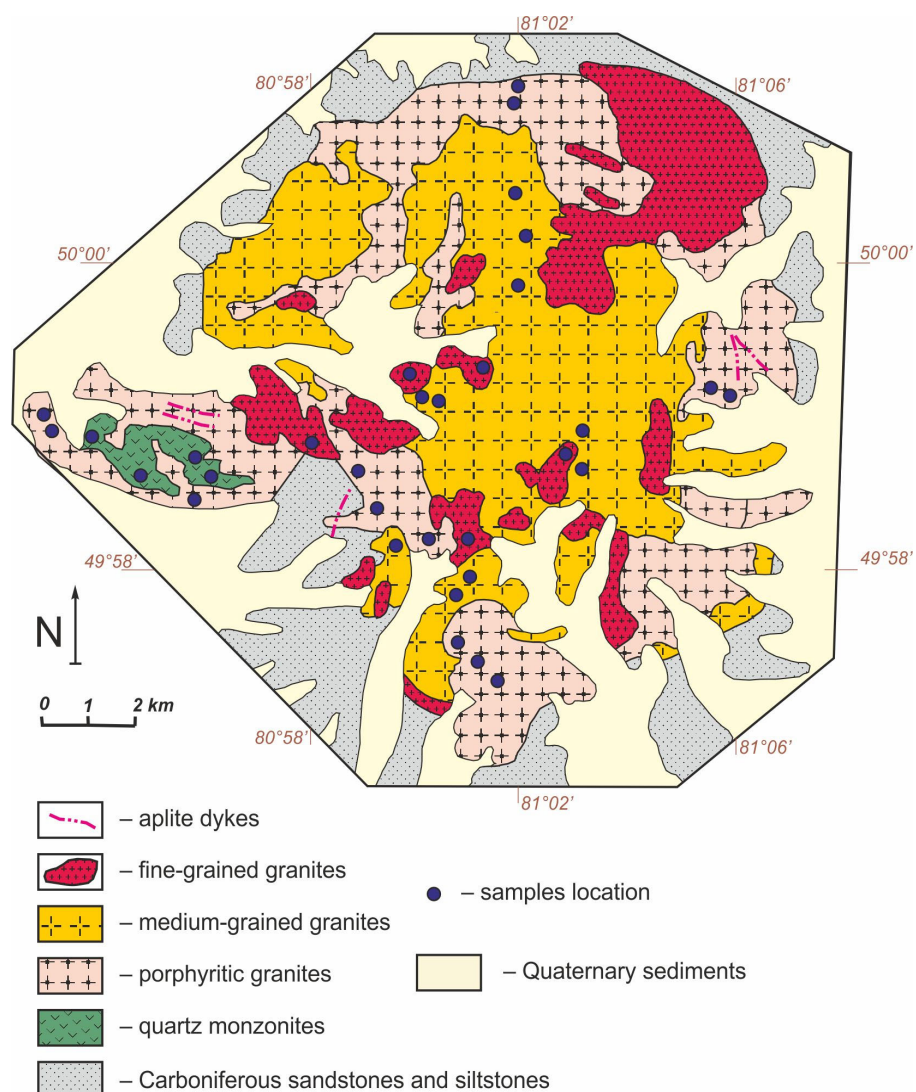
U-Pb dating was performed in the Geothermochronology Center of Kazan Federal University. Each sample weighing about 3 kg was subjected to heavy mineral concentration using a simple flowsheet including methods of gravity and magnetic separation. The heavy mineral fraction was then further isolated using HPS-W (heavy low-viscosity concentrated aqueous solution of sodium heteropolyoxotungstate) at 2.9 g/mL. Zircon grains were hand-picked from the non-magnetic heavy fraction using a ZEISS Stemi DV4 microscope. The grains were mounted in an epoxy resin and then polished for about one half of their thickness. The cathodoluminescence (CL) images of all mounted grains were obtained using a ZEISS Axio Lab A1 microscope with CITL MK5-2 cathodoluminescent attachment to reveal the internal structure of the zircon. U-Pb dating of single zircon grains was measured by the LA-ICP-MS method using an iCAP Qc quadrupole inductively coupled plasma mass spectrometer (ThermoFisher Scientific, Germany) coupled to an Analyte Excite 193 nm excimer based laser ablation system (Teledyne Cetac Technologies). The signals of ^{202}Hg, ^{204}(Pb + Hg), ^{206}Pb, ^{207}Pb, ^{208}Pb, ^{232}Th, and ^{238}U masses were acquired. The ^{235}U signal is calculated from ^{238}U based on the ratio ^{238}U/^{235}U = 137.818 [57]. Analyses

were carried out using spot sizes of 35 μm, a repetition rate of 5 Hz, and a laser fluence of 2.5–3.0 J/cm^2. The data were processed using the software package Iolite 3.65 [58]. Plešovice with the age of 337 Ma [59] was used as the external standard to correct for mass bias, instrument drift, and downhole fractionation of Pb from U during laser drilling. The 91,500 zircon (1065 Ma [60]) was used as secondary standard. During one sample, eight Plesovice standards and eight 91500 standards were measured. Age was calculated, not including a common Pb correction. The construction of concordia diagrams was prepared using the Isoplot 4.15 software package by [61]. All uncertainties are reported at the 2σ level.

The suitability of samples for analyses was confirmed petrographically in transparent thin sections using a Carl Zeiss AxioScope.A1 polarized light microscope equipped with a Canon EOS 650D camera in IGM SB RAS (Novosibirsk, Russia).

The compositions of Semeitau massif rocks were determined at the Center of Geothermochronology of Kazan Federal University, with elemental composition on an S8 Tiger X-ray fluorescence wave-dispersive spectrometer (Bruker, Germany). The analysis of the prepared sample was carried out using the standardized "Geoquant" technique. Trace element compositions of the samples were analyzed on inductively coupled plasma mass spectrometer iCAP Qc (ThermoFisher Scientific, Bremen, Germany). Samples weighing 100 mg each were decomposed in a Teflon autoclave with the addition of hydrochloric, hydrofluoric, nitric, and boric acids in a Microwave Digestion System Ethos up (Milestone, Italy). After cooling the autoclaves, the resulting solution was made up to 50 mL with deionized water. The solution was analyzed on a mass spectrometer pre-calibrated with multielement standards with a concentration in the range of 1 to 100 ppb of each element. The obtained concentration values were recalculated to the initial concentration with considering the empty sample, sample mass and dilution of the solution. The compositions of Delbegetei massif rocks were determined at the Analytical Center for Multi-Elemental and Isotope research SB RAS (IGM, Novosibirsk). Major oxides were analyzed by the X-ray fluorescence (XRF) method using an Applied Research Laboratories ARL-9900-XP analyzer, following the standard procedure. Trace elements were determined by inductively coupled plasma mass spectrometry (ICP-MS) after fusion with LiBO2 on a Finnigan Element high-resolution mass spectrometer. A detailed description of the determination procedure is given in [62].

5. Results

5.1. Petrography of Rocks

The collection of samples from the Semeitau massif includes all types of rocks except for the basalts of the earliest phase and the latest dolerite dikes.

Trachytes (Figure 5a) have about 40 vol.% subhedral phenocrysts. K-feldspar is the predominant phenocryst, accompanied by plagioclase (oligoclase-albite). The rock matrix is composed of microcrystals of potassium feldspar, plagioclase, and quartz.

The rhyolites (Figure 5b) contain about 20–25 vol.% euhedral quartz phenocrysts and rare feldspar phenocrysts within a matrix of felsic volcanic glass.

Monzonites (Figure 5c) are usually porphyritic with a content of early suibidiomorphic plagioclase grains up to 20 vol.%, as well as minerals of later paragenesis—idiomorphic clinopyroxene grains, subidiomorphic plagioclase grains, xenomorphic potassium feldspar grains, subordinate biotite and amphibole. The latest mineral phase is represented by xenomorphic quartz located between early minerals.

Syenites (Figure 5d) are predominantly composed of large subhedral plagioclase and small anhedral grains of K-feldspar, less often xenomorphic late quartz grains. Dark-colored minerals (biotite and amphibole) are present in small amounts.

The porphyritic granosyenites (Figure 5e) contain subhedral phenocrysts of K-feldspar (20 vol.%) and subhedral quartz phenocrysts (up to 10 vol.%) set in a matrix that contains small grains of K-feldspar (predominant), acid plagioclase, and quartz. Dark-colored minerals are almost absent.
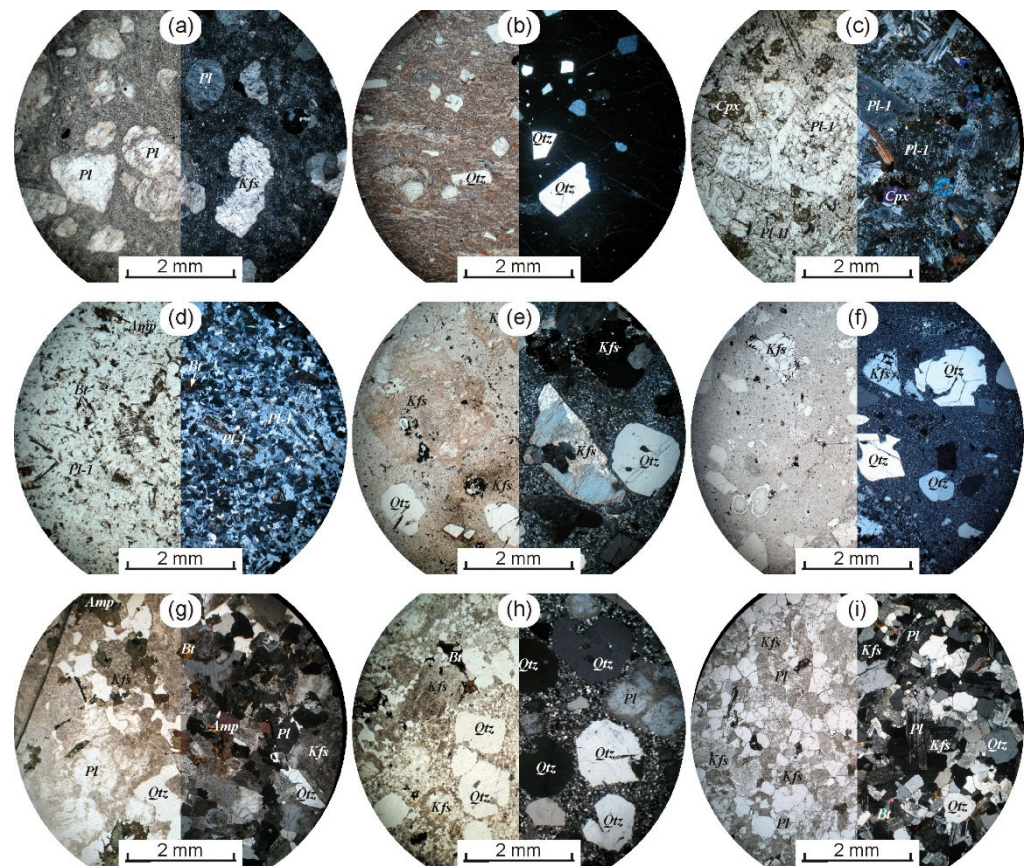
Figure 5. Micro-photos of representative thin sections from the Semeitau (**a**–**f**) and Delbegetei (**g**–**i**) massifs: (**a**) trachyte, (**b**) rhyolite, (**c**) monzonite, (**d**) syenite, (**e**) granosyenite, (**f**) granite, (**g**) quartz monzonite, (**h**) porphyric granite, (**i**) equigranular granite. Mineral symbols: *Pl*, plagioclase; *Kfs*, potassic feldspar; *Qtz*, quartz; *CPx*, clinopyroxene; *Amp*, amphibole; *Bt*, biotite.

The granite porphyries (Figure 5f) are made up of a porphyric texture with subidiomorphic quartz phenocrysts (10 to 20 vol.%) and K-feldspar (7 to 15 vol.%). In addition, commonly, there are fragments of volcanic rocks (granosyenite–porphyries and granite–porphyries). The rock matrix is composed of microcrystals of potassium feldspar, plagioclase, and quartz.

In the Delbegetei massif, all varieties of rocks were studied.

Quartz monzonites (Figure 5g) of the first phase are the medium- and fine-grained rocks consisting of (vol.%) 50–60 plagioclase and K-feldspar, 15–20 euhedral amphibole, 5–10 fine grains of biotite and 15–20 xenomorphic quartz grains.

Almost the entire area of the Delbegetei massif is occupied by fine- or medium-grained granites with a porphyritic texture in the marginal parts and equigranular in the central part of the massif.

Granite with a porphyritic texture (Figure 5h) contains (vol.%) 15–30 subhedral quartz grains, 10–20 K-feldspar, 10–15 albite. For high amounts of quartz crystal (about 25–30 vol.%), most of the studied granites allow us to classify these rocks as leucocratic granites. Fine grains of quartz and feldspar, xenomorphic or poikilitic biotite grains comprise the matrix of these rocks. Biotite is the only dark-colored mineral (up to 5 vol.%).

Equigranular granites (Figure 5i) have an allotriomorphic–granular texture with a content of quartz (25–40 vol.%), potassium feldspar (20–30 vol.%), albite (15–20 vol.%). Due to the high modes of quartz (30–40 vol.%) in most samples, these rocks classify as leucocratic granites. Biotite is the only dark-colored mineral (up to 5 vol.%).

5.2. Zircon U-Pb Geochronology

U-Pb isotope data for zircons from rocks and from standards determined by LA-ICP-MS are available in Supplementary Table S1.

From the center of the southern part of the Semeitau massif, we selected monzonites of the first intrusive phase. All zircons are elongated grains, with length of 300 µm and a width of 50 µm. The prismatic habit predominates, while the bipyramids habit is also common. Cathodoluminescent images of zircons made it possible to determine two types of grains. The first type grains (predominant) have a light gray color in the CL image and a homogeneous internal structure without zoning. The Th/U ratios of these zircon grains range from 1.53 to 1.92. The calculated age shows discordant values (Figure 6a). We assume that the data obtained from these zircons are the result of a disturbance of the U-Pb isotope system (more details in Section 6.3).
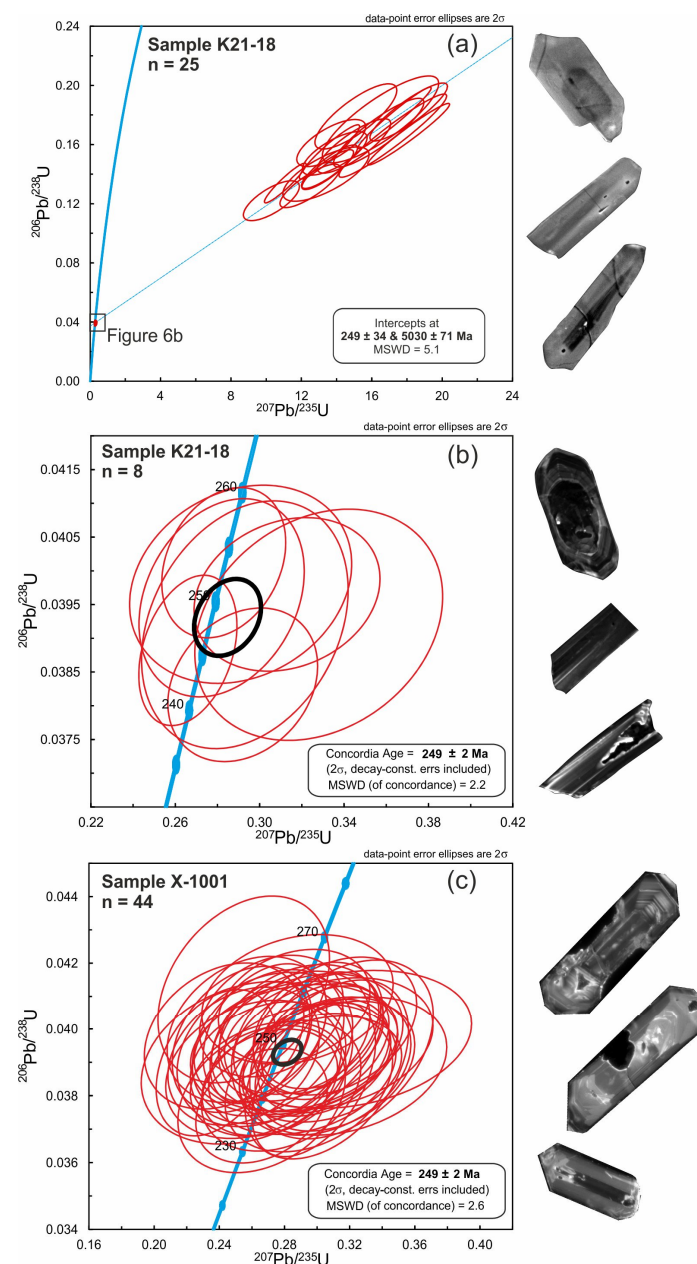

Figure 6. Concordia (Wetherill) diagrams of zircons: (**a**) from the Semeitau massif (1st group of zircons); (**b**) from the Semeitau massif (only 2nd group of zircons); (**c**) from the Delbegetei massif. CL images of simple zircon grains are shown on the right.

Zircon grains of the second morphological type are less common and are oscillatory zoned, which is consistent with their magmatic origin. Zircons of this type have Th/U ratios from 0.54 to 0.91. Their U-Pb concordia age is 249 ± 2 Ma (Figure 6b), which corresponds to the Early Triassic.

From the Delbegetei massif, quartz monzonites of the first phase were selected. Zircon grains are elongated crystals, generally with length of 300 μm and a width of 60 μm, with a prismatic habit, bipyramid and sometimes even pinacoid forms. The magmatic oscillatory zoning is clearly visible in cathodoluminescent images. The resultant concordia age of this zircon grains is 249 ± 2 Ma, an Early Triassic age.

5.3. Major and Trace Element Geochemistry

From the Semeitau massif, 28 rock samples for the content of petrogenic elements and 27 rock samples for the concentration of trace elements were analyzed. From the Delbegetei massif, 50 and 30 rock samples were measured, respectively. Supplementary Table S2 shows the chemical compositions of the studied rocks.

The Semeitau massif rocks on the classification TAS diagram [63] plot in the fields of monzonites, quartz monzonites, syenites and granites (Figure 7a) show a wide range of compositional variations. On the SiO_2-K_2O classification diagram, monzonites, syenites, and trachytes plot to the fields of the shoshonitic series, while felsic rocks plot to the fields of the shoshonitic and high-K calc-alkaline series of rocks (Figure 7c). Different major elemental oxides against SiO_2 content are presented in Figure 8a.
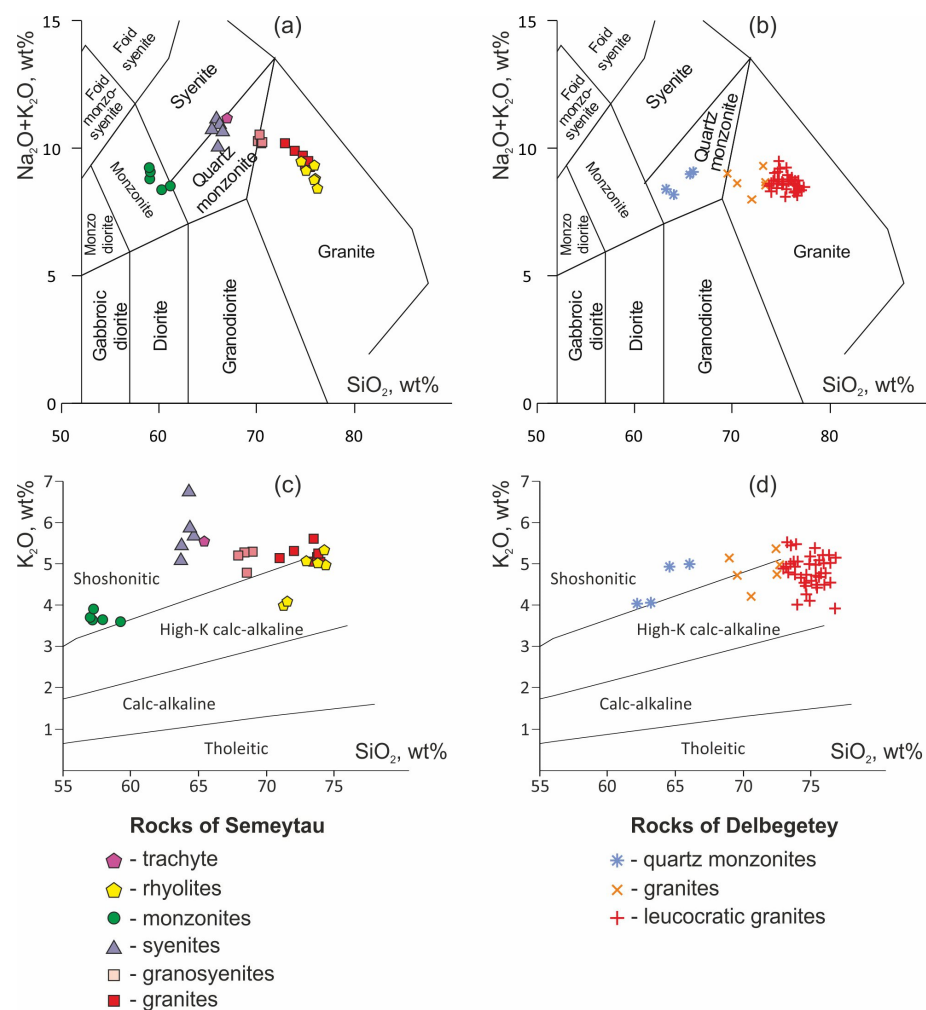

Figure 7. Composition of rocks from the Semeitau and Delbegetei massifs at classification diagrams: (**a**,**b**) alkali versus silica [63]; (**c**,**d**) K_2O versus SiO_2 [64].
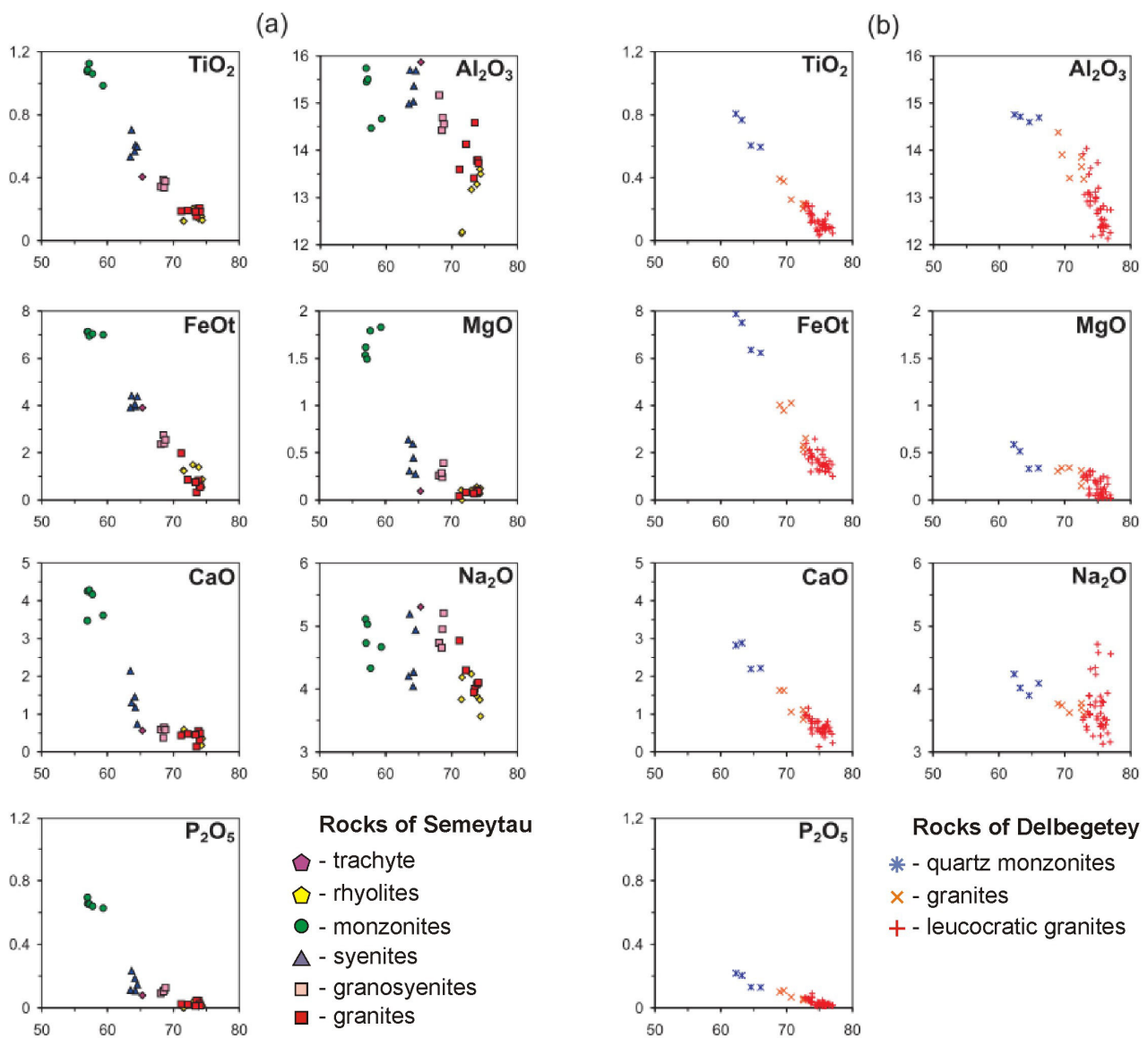
Figure 8. Composition of rocks from the Semeitau (**a**) and Delbegetei (**b**) massifs at binary diagrams "SiO$_2$ vs. major elements oxides".

Monzonites are most mafic rocks (SiO$_2$ = 56.9–59.3 wt%). Compared to other rocks, they have relatively high concentrations of TiO$_2$ (0.99–1.13 wt%), MgO (1.49–1.83 wt%), FeOtot (6.94–7.13 wt%), CaO (3.47–4.28 wt%), and P$_2$O$_5$ (0.63–0.7 wt%), as well as the domination of Na$_2$O over K$_2$O (K$_2$O/Na$_2$O = 0.71–0.85). Syenites are characterized by SiO$_2$ values from 63.5–64.5 wt%, and highest alkalis contents (K$_2$O + Na$_2$O = 9.65–10.88 wt%) with a slight predominance of K$_2$O (K$_2$O/Na$_2$O = 0.99–1.69). Trachytes of the first igneous stage are similar in geochemical characteristics to syenites by content of SiO$_2$, Al$_2$O$_3$, FeOtot, alkalies and K$_2$O/Na$_2$O ratio (1.05). Granosyenite compositions occupy an intermediate field between syenites and felsic rocks. They have SiO$_2$ = 68.1–68.8 wt%, Na$_2$O + K$_2$O = 9.91–10.26 wt%, Al$_2$O$_3$ = 14.42–15.17 wt%, FeOtot = 2.36–2.75 wt%, CaO = 0.37–0.65 wt%. The felsic rocks of the Semeitau massif are similar in contents of major components: SiO$_2$ (71.5–74.4 wt% in rhyolites and 71.2–74.0 wt% in granites), Al$_2$O$_3$ (12.2–13.6 and 13.4–14.6 wt% respectively), FeOtot (0.55–1.49 and 0.33–1.98 wt%), CaO (0.17–0.60 and 0.14–0.56 wt%), Na$_2$O + K$_2$O (7.88–9.24 and 8.99–9.92 wt%).

The Delbegetei massif rocks on the classification TAS diagram [63] plot in the fields of quartz monzonites and granites (Figure 7b). Quartz monzonites belong to the shoshonitic

association; most of the granite samples correspond to the high-K calc-alkaline rock series (Figure 7d). SiO$_2$ content against different major elements oxides is presented in Figure 8b. Quartz monzonites are characterized by SiO$_2$ values from 62.3 to 66.1 wt%. They differ from other rocks in relatively high concentrations of TiO$_2$ (0.60–0.81 wt%), MgO (0.33–0.59 wt%), FeOtot (6.24–7.88 wt%), CaO (2.19–2.88 wt%), and P$_2$O$_5$ (0.13–0.22 wt%). The felsic rocks can be divided into granites and leucocratic granites. Granites contain SiO$_2$ = 69.0–72.9 wt%, Na$_2$O + K$_2$O = 7.82–9.20 wt%, Al$_2$O$_3$ = 13.4–14.4 wt%, FeOtot = 2.14–4.11 wt%, CaO = 0.86–1.63 wt%. The composition of leucocratic granites is SiO$_2$ = 72.8–77.0 wt%, Na$_2$O + K$_2$O = 7.96–9.36 wt%, Al$_2$O$_3$ = 12.1–14.0 wt%, FeOtot = 1.00–2.59 wt%, CaO = 0.13–1.16 wt%.

In the Semeitau massif, monzonites are enriched in Sr, Ba, and Zr, and felsic rocks show enrichment in Rb, Ce, Th contents relative to other rocks (Figure 9a). In the Delbegetey massif, quartz monzonites also have higher Sr, Ba, and Zr contents relative to other rocks, and leucocratic granites are significantly enriched in Cs, Rb, Y, and Th (Figure 9b).
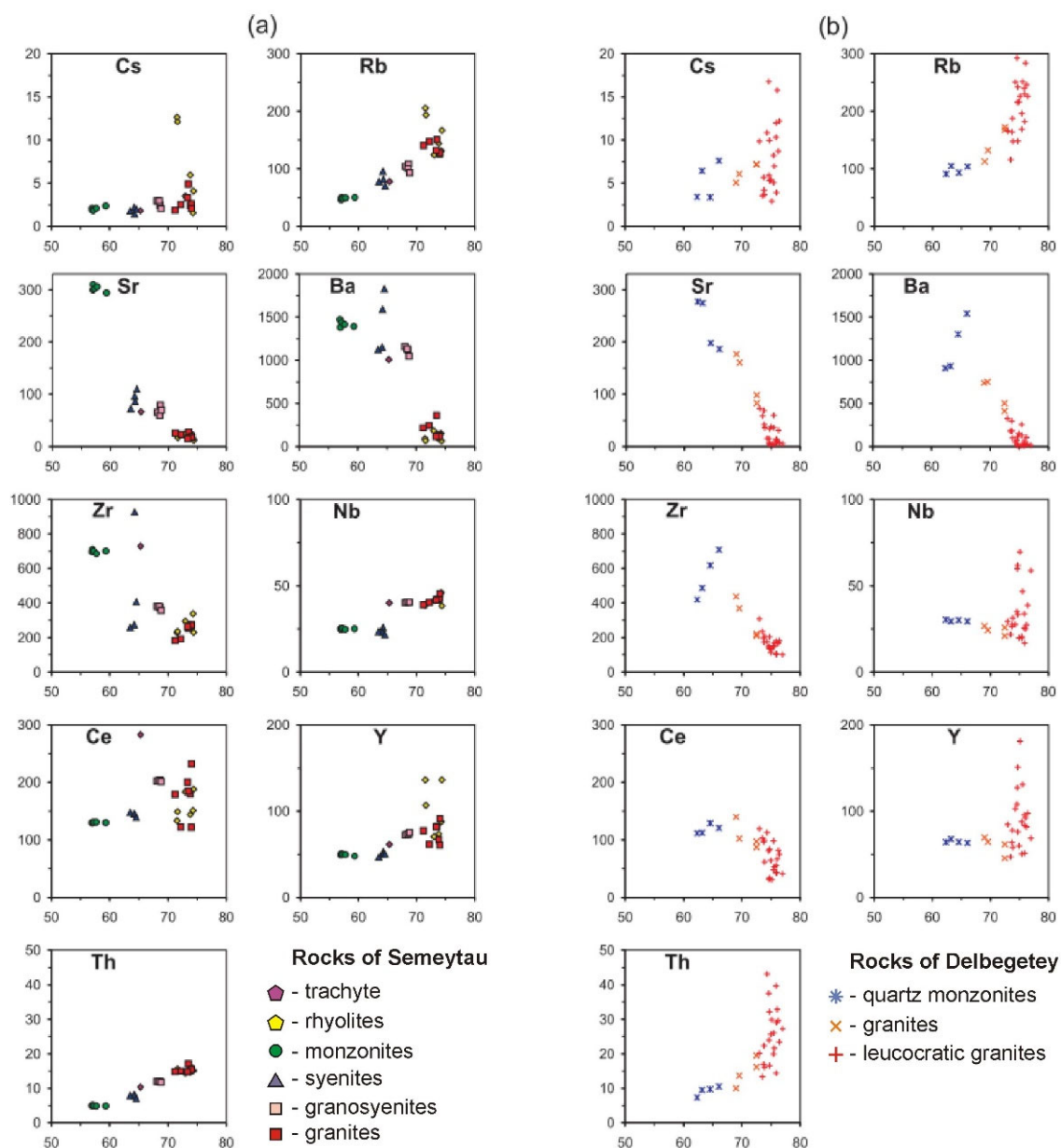

Figure 9. Composition of rocks from the Semeitau (**a**) and Delbegetei (**b**) massifs at binary diagrams "SiO2 vs. trace elements".

REE patterns of Semeitau monzonites have a negative slope (Figure 10, left graphs) and weak negative Eu anomalies (Eu/Eu ∗ N = 0.75–0.77). On a primitive mantle-normalized spider diagrams, monzonite displays positive anomalies in Ba, K and Zr and negative anomalies Sr and Ti. Geochemical behavior of trace elements is similar for syenites and trachytes. REE patterns of trachytes, as well as monzonites, show a weak negative slope and negative Eu anomalies (Eu/Eu ∗ N = 0.36–0.52). On a primitive mantle-normalized spider diagram, trachytes have positive anomalies in K, La, Ce, Nd, Gd and negative anomalies in Ta, Sr, Eu, Ti; syenites have positive anomalies in Ba, K, La, Nd, Gd and negative anomalies in Ta, Sr, Eu, Ti.
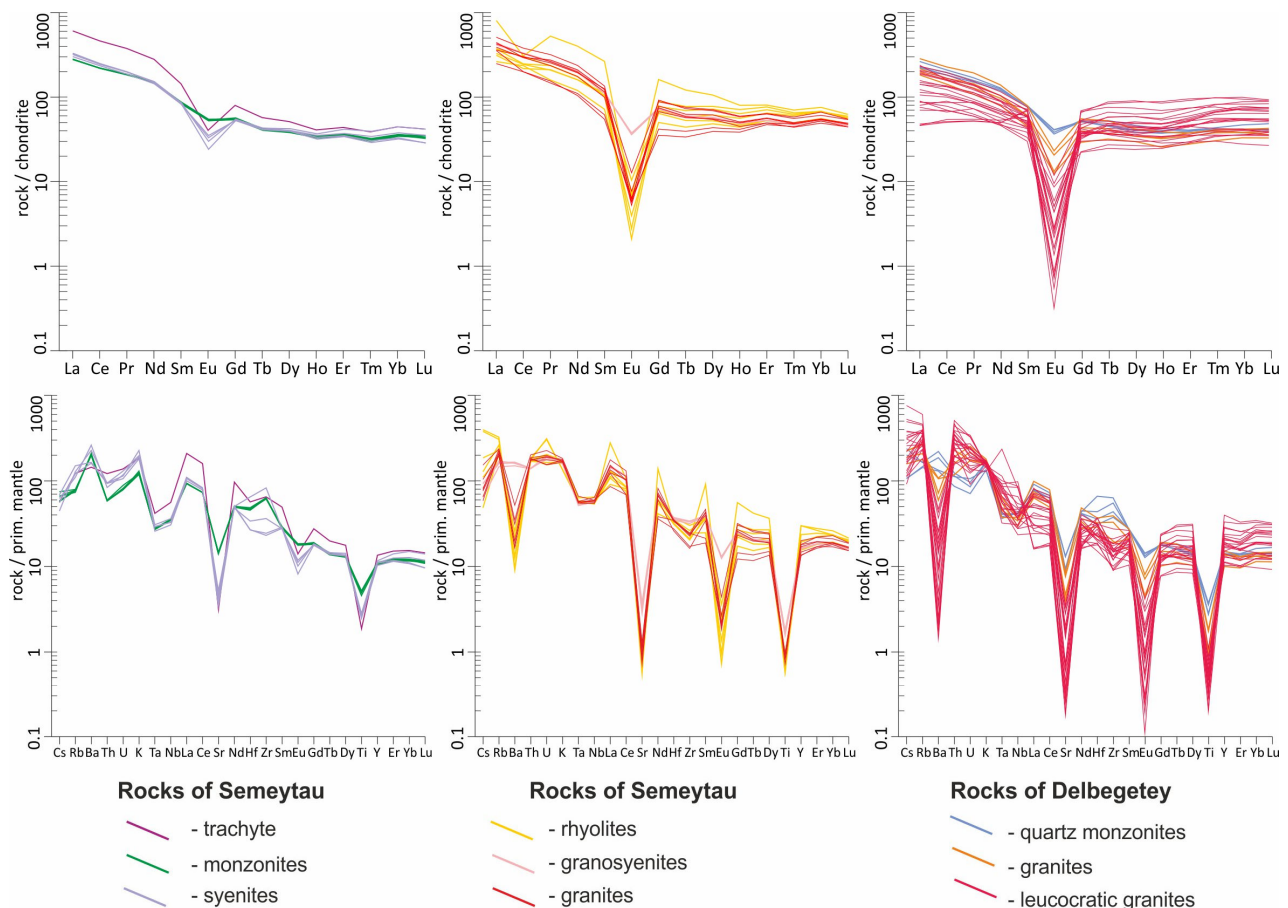

Figure 10. Chondrite-normalized rare earth element patterns (**top**) and primitive mantle-normalized trace element diagrams (**bottom**) for the rocks from the Semeitau and Delbegetei massifs. Normalizing values are from [65].

Felsic rocks of the Semeitau massif demonstrate enrichment in light rare earth element (LREE) concentrations, as well as stronger negative anomalies of indicator elements (Figure 10, graphs in the center). The negative Eu anomalies increase from granosyenites (Eu/Eu ∗ N = 0.39–0.41) to granites (Eu/Eu ∗ N = 0.05–0.14). In rhyolites, there are also strong negative Eu anomalies (Eu/Eu ∗ N = 0.02–0.12). On a primitive mantle-normalized spider diagram, felsic rocks have positive anomalies in Rb, U, La, Nd, Sm and negative anomalies in Sr, Zr, Eu, Ti. Rhyolites and granites also demonstrate the negative Ba anomalies, whereas granosyenites have no Ba anomalies.

In the Delbegetei massif, the REE behavior in quartz monzonites and in granites is similar (Figure 10, right graphs). The chondrite-normalized REE patterns of these rocks have a slight negative slope and weak negative Eu anomalies (Eu/Eu ∗ N = 0.57–0.63 in quartz monzonites and Eu/Eu ∗ N = 0.26–0.40 in granites). Leucocratic granites show almost horizontal REE patterns and strong negative Eu anomalies (Eu/Eu ∗ N = 0.01–0.31).

The primitive mantle-normalized spider diagrams of all rocks of the Delbegetei massif show negative anomalies in Sr, Eu, Ti. The patterns of leucocratic granites show negative Ba and Zr anomalies, whereas quartz monzonites and granites have either positive or an absence of anomalies for these elements.

Comparison of the behavior of the main and rare elements showed the similarity of the composition of the felsic rocks of both massifs. According to the granitoid classification [66], they are ferruginous (Figure 11a) and have high alkalinity (Figure 11b). By the ratio of alumina, calcium and alkalis, most of their compositions correspond to peraluminous (Figure 11c). The high iron-enrichment and alkalinity of granitoid rocks allows us to assume that they belong to A-type granitoids. In the tectonic discrimination diagram [67], most felsic rocks, with the exception of three samples of the Delbegetey massif, plot entirely within the field A-type granites (Figure 11d). On the discrimination diagram [68], the compositions of all studied felsic rocks fall within the field of A_2-type granites (Figure 11e).
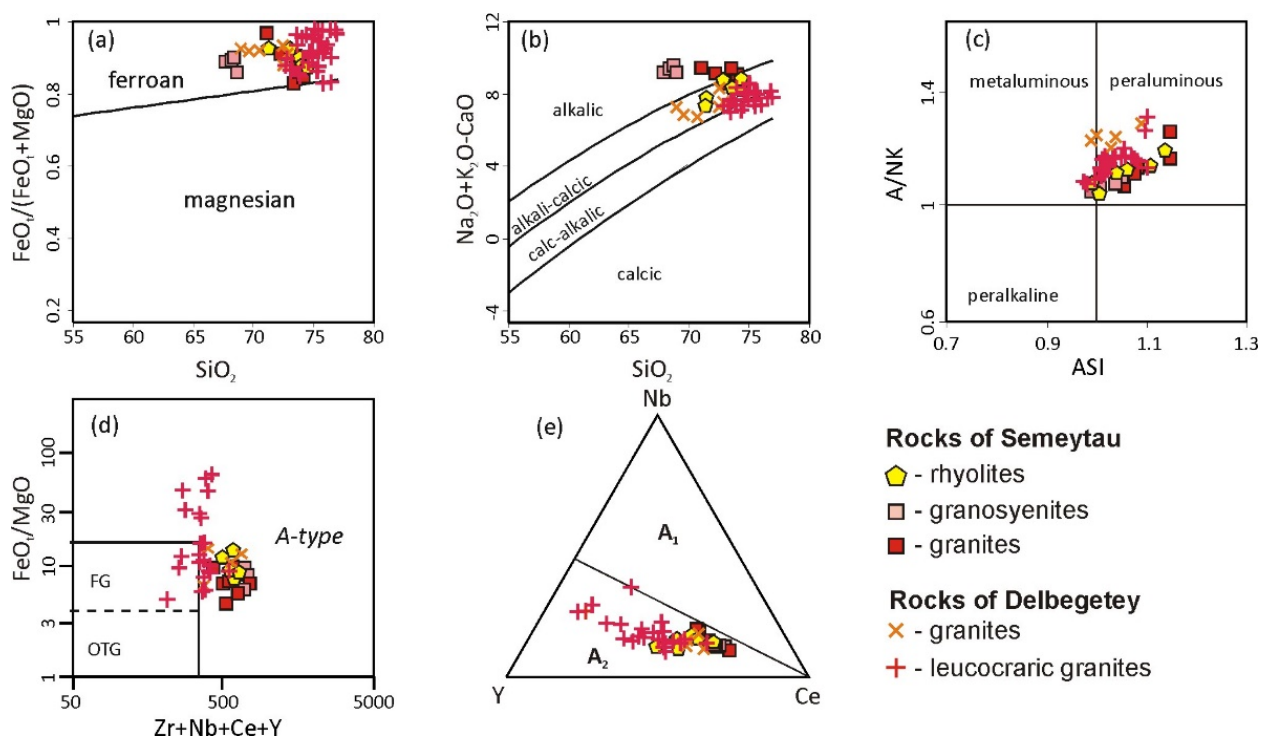

Figure 11. Composition of felsic rocks from the Semeitau and Delbegetei massifs on discrimination diagrams. (**a**): SiO_2 vs. FeOtot/(FeOtot + MgO) [65]; (**b**): SiO_2 vs. MALI [66]; (**c**): Al_2O_3 /($Na_2O + K_2O$) vs. ASI, molecular amounts [66]; (**d**): (Zr + Nb + Ce + Y) vs. FeOtot /MgO [67]; (**e**): Y vs. Nb vs. Ce, ppm [68].

6. Discussion

6.1. Former Opinions

It was previously believed that the Semeitau and Delbegetei massifs belong to different igneous formations and appeared at different stages of the geodynamic evolution of the region [14,55,56].

Based on the predominance of rocks with porphyritic texture, the Semeitau massif has traditionally been ranked as a volcanic structure. Traditionally, the Semeitau massif was considered as a Triassic volcanic structure. The main arguments for this are the predominance of rocks with a porphyritic texture, as well as the interbedding of volcanic rocks of the first igneous stage with tuffs that contain siltstones layers with Triassic flora. The Triassic age has also been confirmed by Ar-Ar dating of sanidine phenocrysts from rhyolites of the first magmatic stage [13]. The formation of this volcanic structure, by

analogy with rift volcanic formations at the base of the West Siberian basin, has been associated with within-plate activity under the influence of the Siberian mantle plume [5] (see Figure 1).

The Delbegetei massif composed of various granitoids of different ages was described as a polychronous massif. The age of massif was estimated as Late Carboniferous and Middle Permian [55]. The formation of the Delbegetei massif was connected with collisional processes that took place in Kazakhstan in the Late Paleozoic [17,55]. It was believed that the Delbegetei massif is the same as massifs of Kalba complex granites that are widespread in Eastern Kazakhstan (see Figure 2).

Our geochronological results, although limited in number, confirm the synchronous crystallization of the two massifs in the Early Triassic, which allows us to consider their formation as a result of similar processes.

6.2. Petrogenesis of Igneous Rocks

Unfortunately, we were unable to find samples of basalt rocks in the Semeitau massif; thus, in this article, we cannot provide data on the truly mafic rocks of this massif. The most mafic rocks are monzonites. Based on the geochemical characteristics of monzonites (SiO_2: 56.9–59.3 wt%; TiO_2: 0.99–1.13 wt%; FeOtot: 6.9–7.1 wt%; CaO: 3.5–4.3 wt%; Sr: 290–310 ppm), we propose that the formation of these rocks formed as the result of the differentiation of mafic magmas. Major and trace element variations are illustrated in binary diagrams in (Figures 8a and 9a). From monzonites to syenites TiO_2, FeOtot, MgO, CaO, P_2O_5, Sr, Ba, Zr abundances decrease with increasing SiO_2, whereas Al_2O_3, Na_2O, Rb increases. This fact indicates that syenites are formed due to the differentiation of monzonite magmas during the fractionation of Fe-Ti oxides, clinopyroxene, apatite, and zircon. Trachytes have the same geochemical characteristics as syenites. It can be assumed that trachytes also are formed due to the differentiation of mafic magmas (basalts of the first phase).

The felsic rocks of the Semeitau massif are similar both in structure and composition. TiO_2, FeOtot, Al_2O_3, Na_2O abundances decrease with increasing SiO_2, whereas Cs, Rb, Zr, Nb, Y, Th increase (Figures 8a and 9a). This confirms the fractionation of plagioclase during the formation of silicic magmas (rhyolites and granites). The behavior of their major and rare elements indicates that these rocks are not a product of differentiation of mafic magmas. Most likely, they are the result of partial melting of crustal substrates. At the same time, granosyenites occupy an intermediate field between syenites and felsic rocks in terms of the contents of major and rare elements (Figures 8a and 9a). This is confirmation of the mixing of mafic magmas with silicic melts with the formation of rocks in composition.

In the Delbegetei massif, quartz monzonites are the most mafic rocks, similar in chemical composition (Figures 8b and 9b) to the syenites of the Semeitau massif. High concentrations of TiO_2, FeOtot, CaO, Sr, Ba, Zr indicate that they are formed due to the differentiation of mafic magmas during the fractionation of Fe-Ti oxides, clinopyroxene, apatite, which is similar to Semeitau syenites formation. In the granites of the Delbegetei massif, TiO_2, FeOtot, Al_2O_3, CaO, Na_2O, P_2O_5, Sr, Ba, Zr, Ce abundances decrease with increasing SiO_2, whereas Cs, Rb, Nb, Y, Th increase (Figures 8b and 9b). This indicates the fractionation of plagioclase, K-feldspar, apatite, and zircon during the formation of silicic magmas. Similar to the felsic Semeitau rocks, the Delbegetei granites, most likely, are the result of partial melting of crustal substrates.

Thus, two genetic groups of rocks are distinguished in both massifs: (1) mafic and intermediate rocks, which are the result of mafic magmas differentiation; (2) felsic rocks, which are the result of crustal substrates melting (with the participation of mafic magmas) and subsequent differentiation toward the most silicic varieties. However, the differences are that in the Semeitau massif, the rocks of the mafic group are more diverse, while in the Delbegetei massif, the products of mafic magmas differentiation are insignificant.

The igneous rocks of the massifs can be attributed to the subalkaline monzonite–granite series with a predominance of felsic rocks. Based on the geological structure of the massifs and the chemical composition of the rocks, we can suppose a model for their formation.

At the first stage, mafic magmas were formed in the lithospheric mantle. The studied monzonites have high concentrations of LREE, K, P, Zr. The appearance of subalkaline monzonites are classified as the result of mixing of primary mafic magmas with crustal substrates or with crustal melts. Others have proposed that the monzonite magmas resulted from partial melting of metasomatized mantle sources [69,70]. Isotope data could be a solution to this problem, but unfortunately, we do not have it yet. This should be a subject for our future research.

Furthermore, the formed monzonite magmas rose to the crust levels, where they were fractionated and interacted with crustal substrates or with crustal melts.

The impact of mafic and monzonite magmas on crustal terrigenous substrates caused their partial melting with the formation of felsic melts. Felsic rocks of both massifs are characterized by high Fe# and enrichment of Zr, Nb, Ce, Y (see Figure 11), which is typical of A-type granites. The partial melting of crustal rocks is a fundamental mechanism for the emplacement of A-granites [68,71,72]. For the studied felsic rocks, strong negative anomalies are observed in the concentrations of Ba, Sr, Eu, which directly indicate the presence of plagioclase (Sr and Eu concentrator) and potassium feldspar (Ba concentrator) in the restite. In this case, it can be assumed that the crustal melts were enriched in silica during melting. Experimental studies on the various substrates melting show the possibility of the enriched in silicic felsic melts formation at low-degree melting [73].

The presence of granosyenites with geochemical characteristics between granites and syenites (Figures 8a and 9a) suggests that there was a partial mixing of monzonite–syenite magmas with crustal silicic melts. Similar models for the syenite–granite series formation were proposed for Western Transbaikalia [74].

The massifs were formed at near-surface levels of the crust. In the Semeitau massif, the intrusion of intrusive phases of different compositions occurred after volcanic eruptions, while the Delbegetei massif was formed during the intrusion of monzonite and granite intrusive phases. Since in Semeitau, mafic and intermediate rocks are present in greater quantities, as well as the volume of magmatism products, it can be assumed that the scale of the processes of crust–mantle interaction and the volume of mafic magmas intruded into the crust were more significant here than in the Delbegetei massif.

6.3. The Age of Massifs

Geochronological data from Semeitau syenites determined two groups of zircons with different ages. For zircons of the first group, the strong discordant age values were obtained with an upper intercept of 5030 ± 71 Ma. The zircons are a well habit and are not rounded; it is doubtful that they are xenocrysts. In addition, these zircons practically do not contain any cores, and discordant ages were obtained mainly from the rims of the grains.

The presence of Proterozoic or Archean zircon cores in the rocks of the Semeytau massif is generally unlikely, since the Precambrian terranes are rare within the CAOB, and the oldest recorded ages do not exceed 2.5 Ga [75,76]. Moreover, the geological structure of Eastern Kazakhstan was generally formed in the Middle–Late Paleozoic on the juvenile crust of the Paleo Asian ocean [17–19] etc., and thus far, no evidence of the presence of Proterozoic or even older zircons has been obtained here.

Thus, we assume that the discordance of the first zircon group is due to the disturbance of the U-Pb isotope system as a result of magmatic or post-magmatic processes (possible interaction with fluids). Some grains probably preserved the U-Pb system undisturbed; they belong to the second group of zircons. The reasons for the disturbance of the U-Pb isotope system can be determined by geochemical studies of zircons and other accessory minerals, as well as by isotopic studies of rocks. We plan to make it in the near future. Thus far, we can assume the age of syenites of the Semeytau massif based on the dating of grains of zircons of the second group at 249 ± 2 Ma. The age of volcanic rocks in the Semeitau

massif (249–248 Ma) was previously determined [13] by Ar-Ar isotope dating of sanidine phenocrysts from trachyte (3 determinations) and rhyolite (2 determinations). Thus, in the Semeitau massif, volcanic and intrusive stages occurred almost simultaneously. The age of Delbegetei quartz monzonites was determined from zircon grains with an undisturbed U-Pb system at 249 ± 2 Ma. The obtained data coincide within the analytical error, which confirms the synchronization of the crystallization of intermediate rocks of both massifs.

The felsic rocks in Semeitau and Delbegetei massifs may be younger than mafic rocks. The age of felsic rocks has not yet been determined by U-Pb dating. However, there are arguments that allow us to consider that they also have an Early Triassic age: (1) felsic rocks are closely associated with intermediate rocks within the massifs, which made it possible to propose a common model of formation (see above); (2) felsic rocks, similar to those in the Semeitau and Delbegetei massifs, do not form independent massifs; (3) in Eastern Kazakhstan, igneous rocks with an age younger than the Early Triassic are still not known.

Thus, we assume that the Semeitau and Delbegetei massifs were formed in the Early Triassic as a result of a single thermal event of the mantle–crustal interaction. The duration of the massifs formation hardly exceeded the first million years.

6.4. Geodynamic Setting

In both massifs, the intermediate rocks are products of differentiation of subalkaline mafic magmas, while the felsic rocks correspond to A-type granites. These geochemical characteristics are an indicator of the intraplate setting. The geological history of the development of the territory of East Kazakhstan also testifies in favor of the within-plate setting [15,16,18,20]: active accretionary–collisional processes in this territory occurred during the Carboniferous, post-orogenic processes actively occurred in the Early Permian, and from the Middle Permian, the territory developed in an intracontinental setting. Thus, the formation of monzonite–granite volcanic–plutonic series of the Semeitau and Delbegetei massifs is the result of intraplate endogenous activity.

The most probable source of energy is the impact of a deep mantle plume. In the Early Triassic, a significant territory of Eurasia was exposed to the impact of the mantle plume, and the Siberian Large Igneous Province was formed [3–5]. Large-scale endogenous events began with the largest outpouring of basalts on the Siberian Platform at the Permian–Triassic boundary [4–7]. Further development of the plume–lithospheric interaction led to the development of a wide area of various magmatism as basalts, kimberlites [8,77] and granitoids in the Early–Middle Triassic [10–12] etc.

In recent years, more and more evidence of Permian–Triassic within-plate magmatism has appeared in the southern part of the Siberian large igneous province. Besides the well-known trap formation in the Kuznetsk Basin (see Figure 1, [78,79]), dyke swarms of lamprophyres and subalkaline diorites, intrusive massifs of monzonites and syenites were found within the Altai fold belt [80,81]. Several large intrusions of granites and leucocratic granites of Early Triassic age have also been described within Altai [10,82–85]. In addition, unpublished data by P.D. Kotler indicate that some granite intrusions in northern and northeastern Kazakhstan also have an Early Triassic age. This indicates that the southern boundary of the large Siberian igneous province extends further south than previously thought [5] and crosses into the Paleozoic structures of the Central Asian fold belt.

The Early Triassic intrusions within the CAOB are characterized by the predominance of granitoids over mafic and intermediate rocks. This can be explained by the structure of the lithosphere of the fold-belts, which was formed during the previous accretion–collision processes. A sufficient amount of crustal terrigenous substrate has accumulated here, which easily undergoes partial melting under the influence of mafic magmas. Basaltic magmas themselves can hardly reach the surface due to their greater density. Such ratios of granitoid and mafic magmatism are characteristic of Large Igneous Provinces within folded belts [2,3].

7. Conclusions

1. The synchronous formation in the early Triassic of the Semeitau and Delbegetei massifs in Eastern Kazakhstan, which were previously considered to be of different ages, has been proven.
2. Both massifs are composed of rocks of the same monzonite–granite series of rocks. The formation of this series is the result of the interaction of mafic magmas with crustal melts formed during the melting of terrigenous substrates.
3. Analysis of the geological position, age and composition of the rocks allows us to conclude that the Semeitau and Delbegetei massifs were formed in an intraplate geodynamic setting. The activity of the mantle plume is the most probable reason for their formation.
4. The Semeitau and Delbegetei massifs can be included in the Early Triassic Siberian large igneous province.

References

1. Bryan, S.E.; Ernst, R.E. Revised definition of Large Igneous Provinces (LIPs). *Earth-Sci. Rev.* **2008**, *86*, 175–202. [CrossRef]
2. Ernst, R.E.; Buchan, K.L.; Campbell, I.H. Frontiers in Large Igneous Province research. *Lithos* **2005**, *79*, 271–297. [CrossRef]
3. Ernst, R.E. *Large Igneous Provinces*; Cambridge University Press: Cambridge, UK, 2014; p. 653.
4. Dobretsov, N.L.; Kirdyashkin, A.A.; Kirdyashkin, A.G.; Vernikovsky, V.A.; Gladkov, I.N. Modeling of thermochemical plumes and implications for the origin of the Siberian Traps. *Lithos* **2008**, *100*, 66–92. [CrossRef]
5. Reichow, M.K.; Pringle, M.S.; Al'Mukhamedov, A.I.; Allen, M.B.; Andreichev, V.L.; Buslov, M.M.; Davies, C.E.; Fedoseev, G.S.; Fitton, J.G.; Inger, S.; et al. The timing and extent of the eruption of the Siberian Traps large igneous province: Implications for the end-Permian environmental crisis. *Earth Planet. Sci. Lett.* **2009**, *277*, 9–20. [CrossRef]
6. Saunders, A.; Reichow, M. The Siberian Traps and the End-Permian mass extinction: A critical review. *Chin. Sci. Bull* **2009**, *54*, 20–37. [CrossRef]
7. Sobolev, S.V.; Sobolev, A.V.; Kuzmin, D.V.; Krivolutskaya, N.A.; Petrunin, A.G.; Arndt, N.T.; Radko, V.A.; Vasiliev, Y.R. Linking mantle plumes, large igneous provinces and environmental catastrophes. *Nature* **2011**, *477*, 312–316. [CrossRef]
8. Ivanov, A.V.; He, H.; Yan, L.; Ryabov, V.V.; Shevko, A.Y.; Palesskii, S.V.; Nikolaeva, I.V. Siberian Traps large igneous province: Evidence for two flood basalt pulses around the Permo-Triassic boundary and in the Middle Triassic, and contemporaneous granitic magmatism. *Earth-Sci. Rev.* **2013**, *122*, 58–76. [CrossRef]

9. Vernikovsky, V.A.; Pease, V.L.; Vernikovskaya, A.E.; Romanov, A.P.; Gee, D.G.; Travin, A.V. First report of early Triassic A-type granite and syenite intrusions from Taimyr: Product of the northern Eurasian superplume? *Lithos* **2003**, *66*, 23–36. [CrossRef]

10. Dobretsov, N.L.; Vladimirov, A.G.; Kruk, N.N. Permian–Triassic magmatism in the Altai-Sayan Fold System as a reflection of the Siberian superplume. *Dokl. Earth Sci.* **2005**, *400*, 40–43.

11. Vernikovskaya, A.E.; Vernikovsky, V.A.; Matushkin, N.Y.; Romanova, V.I.; Berejnaya, N.G.; Larionov, A.N.; Travin, A.V. Middle Paleozoic and Early Mesozoic anorogenic magmatism of the South Yenisei Ridge: First geochemical and geochronological data. *Russ. Geol. Geophys.* **2010**, *51*, 548–562. [CrossRef]

12. Jahn, B.M.; Litvinovsky, B.A.; Zanvilevich, A.N.; Reichow, M. Peralkaline granitoid magmatism in the Mongolian–Transbaikalian Belt: Evolution, petrogenesis and tectonic significance. *Lithos* **2009**, *113*, 521–539. [CrossRef]

13. Lyons, J.J.; Coe, R.S.; Zhao, X.X.; Renne, P.R.; Kazansky, A.Y.; Izokh, A.E.; Kungurtsev, L.V.; Mitrokhin, D.V. Paleomagnetism of the early Triassic Semeitau igneous series, eastern Kazakstan. *J. Geophys. Res.* **2002**, *107*, 2139. [CrossRef]

14. Dyachkov, B.A.; Mizernaya, M.A.; Kuzmina, O.N.; Zimanovskaya, N.A.; Oitseva, T.A. Tectonics and metallogeny of East Kazakhstan. In *Tectonics Problems of Regional Setting*; IntechOpen Limited: London, UK, 2018; pp. 67–84.

15. D'yachkov, B.A.; Mizernaya, M.A.; Khromykh, S.V.; Bissatova, A.Y.; Oitseva, T.A.; Miroshnikova, A.P.; Frolova, O.V.; Kuzmina, O.N.; Zimanovskaya, N.A.; Pyatkova, A.P.; et al. Geological history of the Great Altai: Implications for mineral exploration. *Minerals* **2022**, *12*, 744. [CrossRef]

16. Zonenshain, L.P.; Kuzmin, M.I.; Natapov, L.M. Geology of the USSR: A Plate Tectonic Synthesis. In *Geodynamic Series 21*; American Geophysical Union: Washington, DC, USA, 1990; p. 242.

17. Vladimirov, A.G.; Kruk, N.N.; Rudnev, S.N.; Khromykh, S.V. Geodynamics and granitoid magmatism of collision orogens. *Russ. Geol. Geophys.* **2003**, *44*, 1321–1338.

18. Vladimirov, A.G.; Kruk, N.N.; Khromykh, S.V.; Polyansky, O.P.; Chervov, V.V.; Vladimirov, V.G.; Travin, A.V.; Babin, G.A.; Kuibida, M.L.; Khomyakov, V.D. Permian magmatism and lithospheric deformation in the Altai caused by crustal and mantle thermal processes. *Russ. Geol. Geophys.* **2008**, *49*, 468–479. [CrossRef]

19. Xiao, W.J.; Huang, B.; Han, C.; Sun, S.; Li, J. A review of the western part of the Altaids: A key to understanding the architecture of accretionary orogens. *Gondwana Res.* **2010**, *18*, 253–273. [CrossRef]

20. Khromykh, S.V. Basic and associated granitoid magmatism and geodynamic evolution of the Altai accretion–collision system (Eastern Kazakhstan). *Russ. Geol. Geophys.* **2022**, *63*, 279–299. [CrossRef]

21. Khromykh, S.V.; Kotler, P.D.; Semenova, D.V. Geochemistry, age, and geodynamic settings of formation of the Saur gabbro–granitoid intrusive series (Eastern Kazakhstan). *Geosfernye Issled.-Geosph. Res.* **2019**, *2*, 6–26. [CrossRef]

22. Khromykh, S.V.; Semenova, D.V.; Kotler, P.D.; Gurova, A.V.; Mikheev, E.I.; Perfilova, A.A. Orogenic volcanism in Eastern Kazakhstan: Composition, age, and geodynamic position. *Geotectonics* **2020**, *54*, 510–528. [CrossRef]

23. Khromykh, S.V.; Izokh, A.E.; Gurova, A.V.; Cherdantseva, M.V.; Savinsky, I.A.; Vishnevsky, A.V. Syncollisional gabbro in the Irtysh shear zone, Eastern Kazakhstan: Compositions, geochronology, and geodynamic implications. *Lithos* **2019**, *346–347*, 105144. [CrossRef]

24. Khromykh, S.V.; Kuibida, M.L.; Kruk, N.N. Petrogenesis of high-temperature siliceous melts in volcanic structures of the Altai collisional system of Hercynides (Eastern Kazakhstan). *Russ. Geol. Geophys.* **2011**, *52*, 411–420. [CrossRef]

25. Kuibida, M.L.; Dyachkov, B.A.; Vladimirov, A.G.; Kruk, N.N.; Khromykh, S.V.; Kotler, P.D.; Rudnev, S.N.; Kruk, E.A.; Kuibida, Y.V.; Oitseva, T. Contrasting granitic magmatism of the Kalba fold belt (East Kazakhstan): Evidence for late Paleozoic postorogenic events. *J. Asian Earth Sci.* **2019**, *175*, 178–198. [CrossRef]

26. Khromykh, S.V.; Vladimirov, A.G.; Izokh, A.E.; Travin, A.V.; Prokop'ev, I.R.; Azimbaev, E.; Lobanov, S.S. Petrology and geochemistry of gabbro and picrites from the Altai collisional system of Hercynides: Evidence for the activity of the Tarim plume. *Russ. Geol. Geophys.* **2013**, *54*, 1288–1304. [CrossRef]

27. Khromykh, S.V.; Tsygankov, A.A.; Burmakina, G.N.; Kotler, P.D.; Sokolova, E.N. Mantle-crust interaction in petrogenesis of gabbro-granite association in Preobrazhenka intrusion, Eastern Kazakhstan. *Petrology* **2018**, *26*, 368–388. [CrossRef]

28. Kotler, P.D.; Khromykh, S.V.; Vladimirov, A.G.; Travin, A.V.; Kruk, N.N.; Murzintsev, N.G.; Navozov, O.V.; Karavaeva, G.S. New data on the age and geodynamic interpretation of the Kalba-Narym granitic batholith, Eastern Kazakhstan. *Dokl. Earth Sci.* **2015**, *462*, 565–569. [CrossRef]

29. Kotler, P.D.; Khromykh, S.V.; Kruk, N.N.; Sun, M.; Li, P.; Khubanov, V.B.; Semenova, D.V.; Vladimirov, A.G. Granitoids of the Kalba batholith, Eastern Kazakhstan: U–Pb zircon age, petrogenesis and tectonic implications. *Lithos* **2021**, *388–389*, 106056. [CrossRef]

30. Khromykh, S.V.; Tsygankov, A.A.; Kotler, P.D.; Navozov, O.V.; Kruk, N.N.; Vladimirov, A.G.; Travin, A.V.; Yudin, D.S.; Burmakina, G.N.; Khubanov, V.B.; et al. Late Paleozoic granitoid magmatism of Eastern Kazakhstan and Western Transbaikalia: Plume model test. *Russ. Geol. Geophys.* **2016**, *57*, 773–789. [CrossRef]

31. Khromykh, S.V.; Volosov, A.S.; Kotler, P.D.; Semenova, D.V.; Alexeev, D.V.; Kulikova, A.V. Mafic dike belts in Zharma zone of Eastern Kazakhstan: Position, age and geodynamic implication. *Vestn. D. Serikbaev Ektu* **2021**, *4*, 15–32. [CrossRef]

32. Khromykh, S.V.; Vishnevskiy, A.V.; Kotler, P.D.; Antsiferova, T.N.; Semenova, D.V.; Kulikova, A.V. The Kalba batholith dyke swarms (Eastern Kazakhstan): Mafic magmas effect on granite formation. *Lithos* **2022**, *426–427*, 106801. [CrossRef]

33. Mao, J.W.; Pirajno, F.; Zhang, Z.H.; Chai, F.M.; Wu, H.; Chen, L.S.; Yang, J.M.; Zhang, C.Q. A review of the Cu-Ni sulphide deposits in the Chinese Tianshan and Altay orogens (Xinjiang Autonomous Region, NW China): Principal characteristics and ore forming processes. *J. Asian Earth Sci.* **2008**, *32*, 184–203. [CrossRef]

34. Chen, J.F.; Han, B.F.; Ji, J.Q.; Zhang, L.; Xu, Z.; He, G.Q.; Wang, T. Zircon U-Pb ages and tectonic implications of Paleozoic plutons in northern West Junggar, North Xinjiang, China. *Lithos* **2010**, *115*, 137–152. [CrossRef]

35. Konopelko, D.L.; Biske, Y.S.; Kullerud, K.; Seltmann, R.; Divaev, F.K. The Koshrabad granite massif in Uzbekistan: Petrogenesis, metallogeny, and geodynamic setting. *Russ. Geol. Geophys.* **2011**, *52*, 1563–1573. [CrossRef]

36. Konopelko, D.; Wilde, S.A.; Seltmann, R.; Romer, R.L.; Biske, Y.S. Early Permian intrusions of the Alai range: Understanding tectonic settings of Hercynian post-collisional magmatism in the South Tien Shan, Kyrgyzstan. *Lithos* **2018**, *302–303*, 405–420. [CrossRef]

37. Seltmann, R.; Konopelko, D.; Biske, G.; Divaev, F.; Sergeev, S. Hercynian postcollisional magmatism in the context of Paleozoic magmatic evolution of the Tien Shan orogenic belt. *J. Asian Earth Sci.* **2011**, *42*, 821–838. [CrossRef]

38. Biske, Y.S.; Konopelko, D.L.; Seltmann, R. Geodynamics of late Paleozoic magmatism in the Tien Shan and its framework. *Geotectonics* **2013**, *47*, 291–309. [CrossRef]

39. Shen, P.; Pan, H.; Xiao, W.; Chen, X.; Seitmuratova, E.; Shen, Y. Two geodynamic–metallogenic events in the Balkhash (Kazakhstan) and the West Junggar (China): Carboniferous porphyry Cu and Permian greisen W-Mo mineralization. *Int. Geol. Rev.* **2013**, *55*, 1660–1687. [CrossRef]

40. Zhang, C.L.; Zou, H.B.; Yao, C.Y.; Dong, Y.G. Origin of Permian gabbroic intrusions in the southern margin of the Altai Orogenic belt: A possible link to the Permian Tarim mantle plume? *Lithos* **2014**, *204*, 112–124. [CrossRef]

41. Gao, R.; Xiao, L.; Pirajno, F.; Wang, G.C.; He, X.X.; Yang, G.; Yan, S.W. Carboniferous–Permian extensive magmatism in the West Junggar, Xinjiang, northwestern China: Its geochemistry, geochronology, and petrogenesis. *Lithos* **2014**, *204*, 125–143. [CrossRef]

42. Yarmolyuk, V.V.; Kuzmin, M.I.; Ernst, R.E. Intraplate geodynamics and magmatism in the evolution of the Central Asian Orogenic Belt. *J. Asian Earth Sci.* **2014**, *93*, 158–179. [CrossRef]

43. Yarmolyuk, V.V.; Kozlovsky, A.M.; Travin, A.V. Late Paleozoic anorogenic magmatism in Southern Mongolia: Evolutionary stages and structural control. *Dokl. Earth Sci.* **2017**, *475*, 753–757. [CrossRef]

44. Kozlovsky, A.M.; Yarmolyuk, V.V.; Kudryashova, E.A.; Salnikova, E.B.; Kotov, A.B.; Plotkina, J.V.; Savatenkov, V.M.; Travin, A.V. Late Paleozoic anorogenic magmatism of the Gobi Altai (SW Mongolia): Tectonic position, geochronology and correlation with igneous activity of the Central Asian Orogenic Belt. *J. Asian Earth Sci.* **2015**, *113*, 524–541. [CrossRef]

45. Jiang, C.Y.; Li, Y.Z.; Zhang, P.B.; Ye, S.F. Petrogenesis of Permian basalts on the western margin of the Tarim basin, China. *Russ. Geol. Geophys.* **2006**, *47*, 237–248.

46. Tian, W.; Campbell, I.H.; Allen, C.M.; Guan, P.; Pan, W.Q.; Chen, M.M.; Yu, H.J.; Zhu, W.P. The Tarim picrite-basalt-rhyolite suite, a Permian flood basalt from northwest China with contrasting rhyolites produced by fractional crystallization and anatexis. *Contrib. Mineral. Petrol.* **2010**, *160*, 407–425. [CrossRef]

47. Yu, X.; Yang, S.F.; Chen, H.L.; Chen, Z.Q.; Li, Z.L.; Batt, G.E.; Li, Y.Q. Permian flood basalts from the Tarim Basin, Northwest China: SHRIMP zircon U–Pb dating and geochemical characteristics. *Gondwana Res.* **2011**, *20*, 485–497. [CrossRef]

48. Borisenko, A.S.; Sotnikov, V.I.; Izokh, A.E.; Polyakov, G.V.; Obolensky, A.A. Permo-Triassic mineralization in Asia and its relation to plume magmatism. *Russ. Geol. Geophys.* **2006**, *47*, 170–186.

49. Dobretsov, N.L.; Borisenko, A.S.; Izokh, A.E.; Zhmodik, S.M. A thermochemical model of Eurasian Permo-Triassic mantle plumes as a basis for prediction and exploration for Cu-Ni-PGE and rare-metal ore deposits. *Russ. Geol. Geophys.* **2010**, *51*, 903–924. [CrossRef]

50. Wei, X.; Xu, Y.G.; Feng, Y.X.; Zhao, J.X. Plume-lithosphere interaction in the generation of the Tarim Large Igneous Province, NW China: Geochronological and geochemical constraints. *Am. J. Sci.* **2014**, *314*, 314–356. [CrossRef]

51. Xu, Y.G.; Wei, X.; Luo, Z.Y.; Liu, H.Q.; Cao, J. The Early Permian Tarim Large Igneous Province: Main characteristics and a plume incubation model. *Lithos* **2014**, *204*, 20–35. [CrossRef]

52. Yu, X.; Yang, S.; Chen, H.; Li, Z.; Li, Q. Petrogenetic model of the Permian Tarim Large Igneous Province. *Sci. Chin. Earth Sci.* **2017**, *60*, 1805–1816. [CrossRef]

53. Khromykh, S.V.; Kotler, P.D.; Izokh, A.E.; Kruk, N.N. A review of Early Permian (300–270 Ma) magmatism in Eastern Kazakhstan and implications for plate tectonics and plume interplay. *Geodyn. Tectonophys.* **2019**, *10*, 79–99. [CrossRef]

54. Istomin, A.N.; Salmeneva, I.Z. New data about Early Triassic age of Semeitau voclanic complex. *Izv. AN KazSSR* **1964**, *9*, 86–89. (In Russian)

55. Ermolov, P.V.; Vladimirov, A.G.; Izokh, A.E.; Polyanskii, N.V.; Kuzebnyi, V.S.; Revyakin, P.S.; Bortsov, V.D. *Orogenic Magmatism of Ophiolite Belts (Evidence from Eastern Kazakhstan)*; Nauka: Novosibirsk, Russia, 1983; p. 209. (In Russian)

56. Navozov, O.V.; Solyanik, V.P.; Klepikov, N.A.; Karavaeva, G.S.; Alimkhanov, N.K. Unsolved problems of spatial and genetic relations of mineral deposits with intrusions of the Kalba–Narym and West Kalba zones of the Greater Altai. *Geol. Okhrana Nedr. KazGeo* **2011**, *4*, 66–72. (In Russian)

57. Hiess, J.; Condon, D.J.; McLean, N.; Noble, S.R. $^{238}U/^{235}U$ systematics in terrestrial uranium bearing minerals. *Science* **2012**, *335*, 1610–1614. [CrossRef] [PubMed]

58. Paton, C.; Woodhead, J.; Hellstrom, J.; Hergt, J.; Greig, A.; Maas, R. Improved laser ablation U-Pb zircon geochronology through robust down-hole fractionation correction. *Geochem. Geophys.* **2010**, *11*, Q0AA06. [CrossRef]

59. Slama, J.; Kosler, J.; Condon, D.J.; Crowley, J.L.; Gerdes, A.; Hanchar, J.M.; Horstwood, M.S.A.; Morris, G.A.; Nasdala, L.; Norberg, N.; et al. Plesovice zircon—A new natural reference material for U-Pb and Hf isotopic microanalysis. *Chem. Geol.* **2008**, *249*, 1–35. [CrossRef]

60. Wiedenbeck, M.; Alle, P.; Corfu, F.; Griffin, W.L.; Meier, M.; Oberli, F.; Von Quadt, A.; Roddick, J.C.; Spiegel, W. Three natural zircon standards for U-Th-Pb, Lu-Hf, trace element and REE analyses. *Geostand. Newslett.* **1995**, *9*, 1–23. [CrossRef]

61. Ludwing, K. User's Manual for Isoplot 3.00. In *A Geochronological Toolkit for Microsoft Excel*; Berkeley Geochronology Center: Berkeley, CA, USA, 2003; Volume 4, pp. 1–70.

62. Nikolaeva, I.V.; Palessky, S.V.; Chirko, O.S.; Chernonozhkin, S.M. Determination of major and trace elements by Inductively Coupled Mass-Spectrometry in silicate rocks after fusion with LiBO2. *Anal. I Kontrol (Anal. Control.)* **2012**, *16*, 134–142. (In Russian)

63. Middlemost, E.A.K. Naming materials in the magma/igneous rock system. *Earth Sci. Rev.* **1994**, *37*, 215–224. [CrossRef]

64. Rickwood, P.C. Boundary lines within petrologic diagrams which use oxides of major and minor elements. *Lithos* **1989**, *22*, 247–263. [CrossRef]

65. Sun, S.S.; McDonough, W.F. Chemical and isotopic systematics of oceanic basalts: Implications for mantle composition and processes. *Geol. Soc. Lond. Spec. Publ.* **1989**, *42*, 313–345. [CrossRef]

66. Frost, B.R.; Barnes, C.G.; Collins, W.J.; Arculus, R.J.; Ellis, D.J.; Frost, C.D. A geochemical classification for granitic rocks. *J. Petrol.* **2001**, *42*, 2033–2048. [CrossRef]

67. Whalen, J.B.; Currie, K.L.; Chappell, B.W. A-type granites: Geochemical characteristics, discrimination and petrogenesis. *Contrib. Mineral. Petrol.* **1987**, *95*, 407–419. [CrossRef]

68. Eby, G.N. Chemical subdivision of the A-type granitoids: Petrogenetic and tectonic implications. *Geology* **1992**, *20*, 641–644. [CrossRef]

69. Castro, A.; Aghazadeh, M.; Badrzadeh, Z.; Chichorro, M. Late Eocene–Oligocene post-collisional monzonitic intrusions from the Alborz magmatic belt, NW Iran. An example of monzonite magma generation from a metasomatized mantle source. *Lithos* **2013**, *180–181*, 109–127. [CrossRef]

70. Pontow, R.; Jung, S.; Hauff, F.; Berndt, J. Melting of metasomatically enriched lithospheric mantl—Constraints from Pan-African monzonites (Damara Orogen, Namibia). *Lithos* **2021**, *398–399*, 106332. [CrossRef]

71. Frost, C.D.; Frost, B.R. On ferroan (A-type) granitoids: Their compositional variability and modes of origin. *J. Petrol.* **2011**, *52*, 39–53. [CrossRef]

72. Grebennikov, A.V. A-type granites and related rocks: Petrogenesis and classification. *Russ. Geol. Geophys.* **2014**, *55*, 1074–1086. [CrossRef]

73. Gao, P.; Zheng, Y.F.; Zhao, Z.F. Experimental melts from crustal rocks: A lithochemical constraint on granite petrogenesis. *Lithos* **2016**, *266–267*, 133–157. [CrossRef]

74. Litvinovsky, B.A.; Zanvilevich, A.N.; Wickham, S.M.; Steele, I.M. Origin of syenite magmas in A-type granitoid series: Syenite–granite series from Transbaikalia. *Petrology* **1999**, *7*, 483–508.

75. Degtyarev, K.; Yakubchuk, A.; Tretyakov, A.; Kotov, A.; Kovach, V. Precambrian geology of the Kazakh Uplands and Tien Shan: An overview. *Gondwana Res.* **2017**, *47*, 44–75. [CrossRef]

76. Yarmolyuk, V.V.; Degtyarev, K.E. Precambrian terranes of the Central Asian Orogenic Belt: Comparative characteristics, types, and peculiarities of tectonic evolution. *Geotecton* **2019**, *53*, 1–23. [CrossRef]

77. Sun, J.; Liu, C.Z.; Tappe, S.; Kostrovitsky, S.I.; Wu, F.Y.; Yakovlev, D.; Yang, Y.H.; Yang, J.H. Repeated kimberlite magmatism beneath Yakutia and its relationship to Siberian flood volcanism: Insights from in situ U–Pb and Sr–Nd perovskite isotope analysis. *Earth Planet. Sci. Lett.* **2014**, *404*, 283–295. [CrossRef]

78. Kruk, N.N.; Plotnikov, A.V.; Vladimirov, A.G.; Kutolin, V.A. Geochemistry and geodynamic conditions of the trap rock formation in the Kuznetsk basin. *Dokl. Earth Sci.* **1999**, *369A*, 1387–1390.

79. Buslov, M.M.; Safonova, I.Y.; Fedoseev, G.S.; Reichow, M.K.; Davies, K.; Babin, G.A. Permo-Triassic plume magmatism of the Kuznetsk Basin, Central Asia: Geology, geochronology, and geochemistry. *Russ. Geol. Geophys.* **2010**, *51*, 1021–1036. [CrossRef]

80. Vasyukova, E.A.; Izokh, A.E.; Borisenko, A.S.; Pavlova, G.G.; Sukhorukov, V.P.; Anh, T.T. Early Mesozoic lamprophyres in Gorny Altai: Petrology and age boundaries. *Russ. Geol. Geophys.* **2011**, *52*, 1574–1591. [CrossRef]

81. Krupchatnikov, V.I.; Vrublevskii, V.V.; Kruk, N.N. Early Mesozoic lamproites and monzonitoids of Southeastern Gorny Altai: Geochemistry, Sr-Nd isotope composition, and sources of melts. *Russ. Geol. Geophys.* **2015**, *56*, 825–843. [CrossRef]

82. Vladimirov, A.G.; Ponomareva, A.P.; Shokalsky, S.P.; Khalilov, V.A.; Kostitsyn, Y.A.; Ponomarchuk, V.A.; Rudnev, S.N.; Vystavnoi, S.A.; Kruk, N.N.; Titov, A.V. Late Paleozoic-early Mesozoic granitoid magmatism in Altai. *Russ. Geol. Geophys.* **1997**, *38*, 715–729.

83. Gavryushkina, O.A.; Travin, A.V.; Kruk, N.N. Duration of granitoid magmatism in peripheral parts of large igneous provinces (based on ^{40}Ar/^{39}Ar isotopic study of Altai Permian-Triassic granitoids). *Geodyn Tectonophys* **2017**, *8*, 1035–1047. [CrossRef]

84. Gavryushkina, O.A.; Kruk, N.N.; Semenov, I.V.; Vladimirov, A.G.; Kuibida, Y.V.; Serov, P.A. Petrogenesis of Permian-Triassic intraplate gabbro-granitic rocks in the Russian Altai. *Lithos* **2019**, *326–327*, 71–89. [CrossRef]

85. Vetrov, E.V.; De Grave, J.; Kotler, P.D.; Kruk, N.N.; Zhigalov, S.V.; Babin, G.A.; Fedoseev, G.S.; Vetrova, N.I. Evolution of the Kolyvan-Tomsk granitoid magmatism (Central Siberia): Insights into the tectonic transition from post-collision to intraplate settings in the northwestern part of the Central Asian Orogenic Belt. *Gondwana Res.* **2021**, *93*, 26–47. [CrossRef]